Kent Academic Repository

Full text document (pdf)

Citation for published version

Qin, Fan and Gao, Steven and Luo, Qi and Wei, Gao and Gu, Chao and Xu, Jiadong and Li, Jianzhou and Mao, Chunxu and Wu, Changyin (2017) A Tri-Band Low-Profile High-Gain Planar Antenna Using Fabry-Perot Cavity. IEEE Transactions on Antennas and Propagation, 65 (5). pp. 2683-2688. ISSN 0018-926X.

DOI

https://doi.org/10.1109/TAP.2017.2670564

Link to record in KAR

http://kar.kent.ac.uk/59769/

Document Version

Author's Accepted Manuscript

Copyright & reuse

Content in the Kent Academic Repository is made available for research purposes. Unless otherwise stated all content is protected by copyright and in the absence of an open licence (eg Creative Commons), permissions for further reuse of content should be sought from the publisher, author or other copyright holder.

Versions of research

The version in the Kent Academic Repository may differ from the final published version.
Users are advised to check **http://kar.kent.ac.uk** for the status of the paper. **Users should always cite the published version of record.**

Enquiries

For any further enquiries regarding the licence status of this document, please contact:
researchsupport@kent.ac.uk

If you believe this document infringes copyright then please contact the KAR admin team with the take-down information provided at **http://kar.kent.ac.uk/contact.html**

KAR Kent Academic Repository

University of Kent

A Tri-Band Low-Profile High-Gain Planar Antenna using Fabry-Perot Cavity

Fan Qin, Steven Gao, Qi Luo, Gao Wei, Chao Gu, Jiadong Xu, Jianzhou Li, Chunxu Mao, Changyin Wu

Abstract— A tri-band high-gain antenna with a planar structure and low profile is proposed. The principle of operation is explained. It is based on Fary-Perot cavity antenna (FPCA) with two frequency selective surface (FSS) layers. Two different resonant frequencies are generated by the two resonant cavities formed by the ground plane and each of the two FSS layers, respectively. A third resonant frequency is produced by combining the two FSS layers together. Advantages of this tri-band antenna includes low profile, high gain, easy fabrication and low cost. Low profile is achieved by designing the combined FSS layers as an artificial magnetic conductor (AMC) with a reflection coefficient having 0º phase shift and high magnitude. In addition, a large frequency ratio, which is often a problem for multiband array antennas, can be achieved here. To verify this concept, a C/X/Ku band FPCA is designed and one prototype is fabricated and tested. Experimental results agree well with the simulated results. High gain performance with good impedance matching in three bands is obtained, which reaches a peak gain of 14.2 dBi at 5.2 GHz, 18.9 dBi at 9.6 GHz and 19.8 dBi at 14.7 GHz, respectively. The overall height of antenna is only 20.2 mm, which is about 1/3 wavelength at its lowest operating frequency, which means a reduction of 30% compared to the height of traditional FPCA antenna.

Index Terms—Antenna, low-profile, tri-band, high gain, Fabry-Perot, partially reflective surface, array

I. INTRODUCTION

THE antennas and arrays which have high gain and can operate over multiple frequency bands are of significant interest to wireless industries, due to the large numbers of antennas required to satisfy the requirements of various wireless systems at different frequency bands such as synthetic-aperture radars, satellite communications, Global Navigation Satellite Systems (GNSS), terrestrial mobile communications and deep-space links [1-3]. Several technologies have been used to realize multiband antennas including multi-patch microstrip structure [4], stacked microstrip antenna [5] and multiband slot antenna [6], etc. In addition, to overcome the radio propagation path losses over a long distance, especially in higher frequencies, high gain is also a crucial requirement. Classical antennas such as large reflectors [7], waveguide horns [8], dielectrics lenses [9] and large-scale antenna arrays [10] offer attractive solutions to achieving high gain performance. However, these techniques are limited in some applications due to their design complexity, bulky size, high cost and/or significant power losses in the feed network. Some dual-band high-gain arrays are also reported [1] but they have rather complicated structures. Therefore, it is necessary to investigate novel solutions to multi-band high-gain antennas with planar structures, low profile, simple feed mechanisms and low cost.

FPCA has been widely investigated in recent years due to its high gain, fabrication simplicity, simple feed system and low-cost compared with traditional high-gain antennas [11-13]. A FPCA antenna typically consists of a primary feed antenna located in a resonant cavity formed between a perfect reflector and a partially reflective surface (PRS) , which is usually constructed by a dielectric superstrate or a periodic surface, such as 1-D dielectric slabs, 2-D dielectric grids and rods, 2-D printed frequency selective surfaces (FSSs). The operation of this antenna has been successfully analyzed by a ray optics theory [14]. A significant enhancement of antenna's directivity can be achieved by means of the multiple reflections between the ground plane and the PRS.

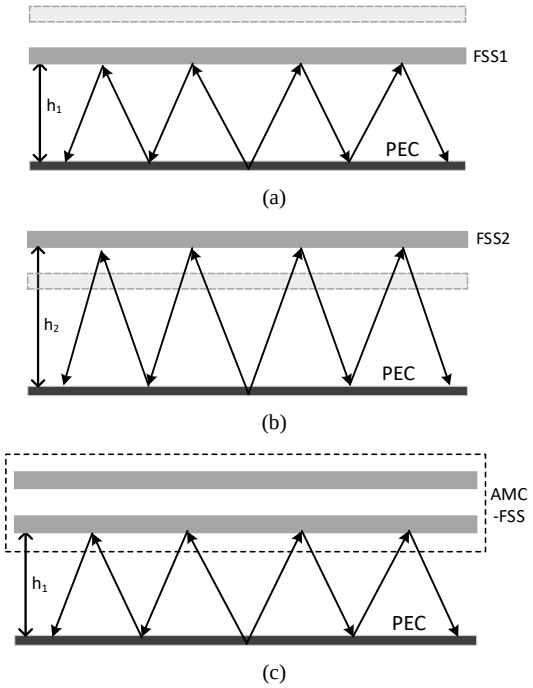

Fig. 1 Resonant cavity formed by a PRS operating in triple-bands: (a) f_1; (b) f_2; (c) f_3

To meet the requirements in different applications, various FPCAs have been implemented so far, including wideband FPCA [15], low-profile FPCA [16] and dual-band FPCA [17]. The cavity height of a conventional FPCA antenna is approximately one half wavelength or more, which is too large for some applications where a low profile is essential. To reduce the height of cavity, an artificial magnetic conductor (AMC) was employed as the ground plane, causing a $\lambda/4$ cavity height [18]. Further reduction of the cavity height was proposed in [19], where a $\lambda/60$ profile was achieved. More recently, a PRS with both properties of high reflection and AMC was employed in

[20], where the low-profile was achieved without additional AMC as the ground plane.

Dual-band FPCAs also attract many interests. A method employing a high impedance surface (HIS) as the ground plane was reported in [21], where two resonant frequencies were generated to achieve dual-band performance. A dual-band FPCA based on inverted reflection phase gradient of the PRS was achieved in [22]. Similar design was reported in [23]. Two identical dielectric slabs were applied to generate the inverted reflection phase gradient of PRS for obtaining the resonances in two different frequencies in this design. In [24], a dual-frequency FPCA was discussed by utilizing the first and second order resonances of the resonant cavity. One limitation of these dual-band FPCAs mentioned above is that it is difficult to design two frequencies independently since the two operating frequencies are affected by each other. This can be overcome by utilizing a double-layer PRS forming two separated resonant cavities [25]. More flexible frequency ratio can be realized using this method. A tri-band FPCA operating at 10.8 GHz, 11.3 GHz and 12.2 GHz was proposed in [26], where a single dielectric layer coated with two same periodic slot arrays on its two sides was employed in this design. To the best of our knowledge, this is the only one public report about tri-band FPCA so far. However, only simulation results of this tri-band FPCA was given in [26] without any validation of results by fabrication and measurement results.

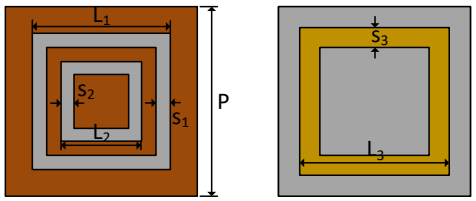

(a) (b)

Fig. 2 The structures of the two FSS structures: (a) structure 1; (b) structure 2

This paper presents our research work on tri-band high-gain FPCA antenna with low profile, planar structure, easy fabrication and low cost. The PRS is formed using two FSS layers with double-ring array and ring-slot array printed on one side of the two dielectric layers. Remarkable enhancement of antenna's directivity is obtained in three bands. The working principle is described. The middle and up frequencies are realized based on the two separated FP resonant cavities formed by the lower and upper FSS layers, respectively. For the low frequency, it is achieved by the two FSS layers together in the same resonant cavity. This combined FSS-layers has the property of AMC and it can produce 0^o reflection phase in low frequency band, resulting in a low cavity profile. Approximately 30% reduction in cavity height is achieved compared with other conventional FPCAs. Another advantage of this antenna is that it can achieve triple-band performance with a large frequency ratio, which is often difficult to be obtained by dual-band or multi-band array antennas.

The paper is organized into the following sections. The working principle and the design of the two FSSs are described in Section II. In Section III, the performance of the tri-band FPCA is simulated with parametric study. The feed antenna design is also shown in this section. A prototype is fabricated and the measured results with simulated ones as comparison are reported in Section IV. Finally, concluding remarks are given in Section V.

II. Design Principle

This section presents the design principle of the tri-band FPCA. Figure 1 shows the side view of the proposed tri-band high-gain antenna. As shown in Fig. 1, there are two FSS layers as the PRS of the proposed antenna. Two resonant cavities with a height of h1 and h2 are formed by the ground plane and the lower or upper FSS layer, respectively. h_1 / h_2. The principle of the FPCA operating at f_1 and f_2 is based on the classical theory of FPCA as reported in [25]. Assuming the cavity 1 and 2 resonate at f_1 and f_2, respectively, the FSS 1 is required to have sufficient reflection magnitude at f_1 and be transparent at f_2, respectively. Likewise, FSS 2 is required to have high reflection magnitude at f_2 and let the electromagnetic wave propagate freely at f_1. To achieve tri-band operation, a possible way is to combine the two FSS layers together as the PRS to obtain the third resonance based on this dual-band FPCA, as shown in Fig.1 (c).

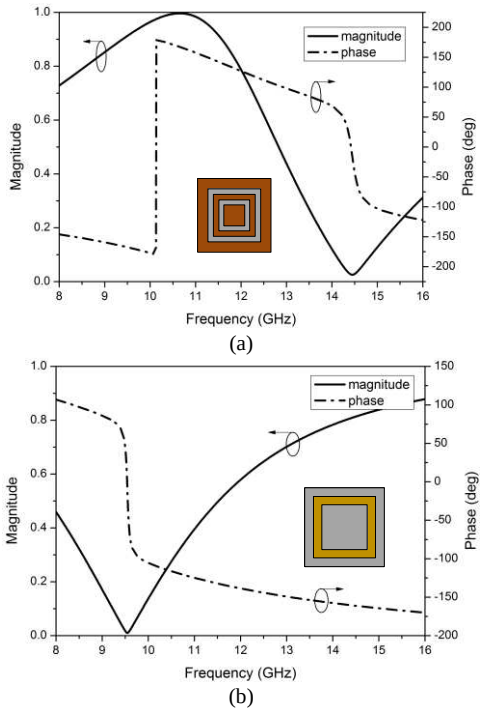

Fig. 3 the reflection coefficients of the two FSSs: (a) structure 1; (b) structure 2

The unit cells of the FSS in our design are shown in Fig. 2. They are printed on one side of 0.8 mm thick dielectric substrate with ε_r=3.55. Two structures are selected as the candidates of the two FSS layers. Structure 1 consists of two metallic rings, as shown in Fig. 2(a). The length of the outer ring is set as L_1 and the inner one is L_2, respectively. The width of the outer and inner rings are S_1 and S_2, respectively. The structure 2 is formed by a ring slot with the length of L_3 and width of S_3, which is shown in Fig. 2 (b). Both of these two structures have the same periodicity P.

To study the reflection coefficient of each FSS structure, full-

wave simulations (CTS Microwave Studio) with the consideration of periodic boundary is employed. The calculated reflection coefficient is shown in Fig. 3 (a) and (b). It can be seen that the electromagnetic wave can pass through the structure 1 freely at 14.5 GHz and it is fully reflected by the one at 10.5 GHz. Meanwhile, a 'zero magnitude' at 9.5 GHz and a sufficient reflection at 14.5 GHz are obtained by the structure 2, respectively. According to the working principle introduced above, dual-band FPCA operating at 9.5 GHz (the cavity formed by structure 1 and ground plane) and 14.6 GHz (the cavity formed by structure 2 and ground plane) can be achieved using these two FSS structures.

The reflection phases of structure 1 and 2 at 9.6 GHz and14.5 are -170° and -161°, which is equivalent to 190° and 199°, respectively. The heights of the FP cavities formed by structure 1 and 2 can be estimated by the following equation

$$h = \frac{\lambda}{4\pi}\left(\varphi_{prs} + \pi\right) + \frac{\lambda}{2} \times N, N = 0,1,2 \ldots \quad (1)$$

where h is the cavity height, λ is the wavelength of the operating frequency, φ_{prs} is the reflection phase of the PRS and π is the reflection phase of the ground plane.

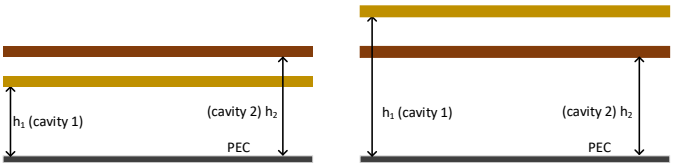

(a) (b)

Fig. 4 two options of the dual-band performance: (a) option 1; (b) option 2

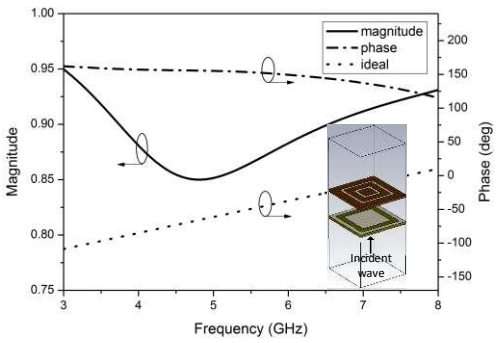

(a)

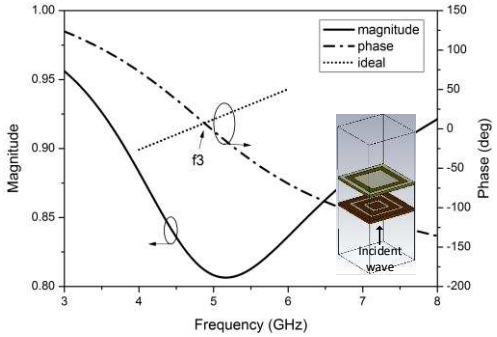

(b)

Fig. 5 Reflection coefficients of the combined-FSS: (a) option 1; (b) option 2

Fig.4 shows the two possible options for forming the two separated FP cavities: the option 1 is that both of the two cavities work at the first order resonant length (N=0). In this case, the FPCA owns the smallest resonant length. The structure 1 is mounted on the top of the second structure with calculated cavity heights: h_1=16 mm and h_2=9.9 mm. For the option 2, the structure 1 keeps working at the first order resonant and the structure 2 is changed to work at the second order resonant, whose cavity height is varied to h_2=20.3 mm (N=1). In this case, the structure 2 is on the top of the structure 1. It should be noted that both of the two options can operate dual-band FPCA at 9.6 GHz and 14.5 GHz.

As mentioned above, the key to achieve tri-band performance for FPCA in Figure 1 is to find a third resonance (f_3) based on the combined two FSS layers. The possibility of the third resonance in these two options are investigated as following. Fig. 5 (a) and (b) present the simulated reflection coefficient of the combined-FSS layer in the case of option 1 and 2, respectively. The ideal phase making the cavity resonate is plotted for finding the third resonance. It can be observed that there is no intersection between the reflection phase of the combined FSS and the ideal phase in option 1, which means the third resonant frequency cannot happen in this case. For the option 2, the reflection phase has the property of AMC, which can produce the zero reflection phase at around 5 GHz. An intersection between the reflection of the combined FSS and ideal phase occurs at 5.1 GHz, which means this combined FSS can satisfy the resonant condition at this frequency. Thus, the third resonance can be found in option 2. Moreover, the reflection magnitude of the combined FSS (over 0.8) is large enough as well, causing a high gain performance at this frequency. The estimated cavity height of h_1 is 16 mm and the whole cavity height is 20.3 mm, which is approximately 1/3 λ at 5.1 GHz. Compared with a conventional FPCA whose cavity height is around half wavelength, a great reduction of the cavity height is obtained. Consequently, three resonances occurring in one FPCA with a low-profile is achieved theoretically utilizing the two combined FSS layers in the case of option 2.

III. Finite-Size Triple-Band FPCA

A. Performance of the Triple-band

To demonstrate the performance of the triple-band FPCA, the antenna's directivity in three operating bands is investigated separately. In addition, since the height of cavity height effects on the performance of FPCA, the parameters of the cavity height (h_1 and h_2) is carefully studied as well. A simple patch antenna placed in the center of the ground plane is modeled to feed the FP cavity. The two FSS layers consisting of 11×11, 7×7 and 5×5 units in C, X and Ku bands are employed, respectively.

Fig. 6 shows the FPCA's directivity with different cavity heights in three bands. It is revealed that the high directivities are obtained in C, X and Ku bands by employing the proposed two FSS layers. The C-band resonant frequency is impacted by both of the two cavity heights as shown in Fig.6 (a). Its resonance moves to lower frequency as h_1 decreases with h_2 unchanged as well as h_2 increases with keeping h_1. This is due to the reason that the reflection phase of the combined FSS, which mainly determines the characteristic of FPCA, is

impacted by the both two FSS layers. To better explain the reason, Fig. 7 plots the parametric study of the spacing between the two FSS layers. The magnitude of the combined FSS can maintain at a high value. The resonant frequency of this combined-FSS, where the zero reflection phase occurs, moves to lower frequency with the increase of the spacing, causing the reflection phase varies with the variation of h_1 or h_2 and leading to the variation of the operating resonant frequency in C band.

Since the other two resonant frequencies are determined by the cavity 1 and 2, respectively, the performance of the X-band resonance (9.6 GHz) and Ku-band resonance (14.6 GHz) is mainly impacted by h_1 and h_2, respectively, as shown in Fig. 6 (b) and (c). The resonances (X and Ku bands) move to lower frequency with the increase of the cavity heights, which keeps consistent with our expectation.

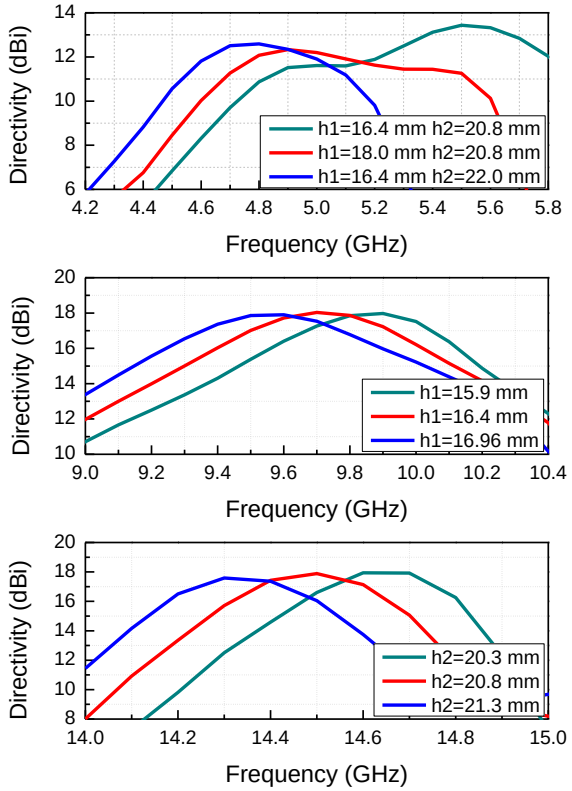

Fig. 6 Directivities in C, X and Ku bands with different cavity heights

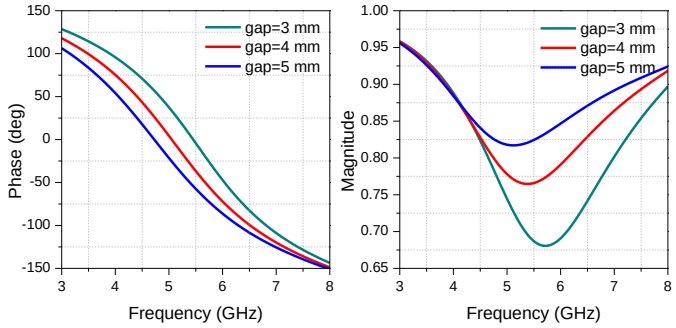

(a) (b)

Fig. 7 Reflection coefficients of the combined-FSS with different spaicing: (a) reflection phase; (b) reflection magnitude

B. Effect of Physical Size on *FPCA's Directivity*

The calculated directivity with different numbers of the FSSs' units in three bands is shown in Fig. 8 (a), (b) and (c), respectively. It is predicted that the directivity increase with enhancing the dimension of the combined FSS. It increases from 11.2 dBi to 14.9 dBi when the units grow from 9×9 to 13×13 in C-band. This value is increased by 3.2 dB when the units increase from 7×7 to 11×11 in X-band. While, when keep increasing the units, little enhancement of the directivity occurs in Ku band. This is because the aperture of the combined FSSs is large enough for the Ku-band and the reflected wave from the edges of superstrate has little contribution to antenna's directivity. It should be noted that the 3-dB directivity radiation decrease as the aperture increases since more non-uniform filed distribution occurs on larger aperture, which deteriorate the 3-dB radiation bandwidth. This phenomenon also can be expected in C and X bands if the units keep growing. Thus, for a conventional FPCA, although higher directivity can be obtained using larger aperture, it deteriorates 3-dB radiation bandwidth. On the other hand, small aperture has limited directivity enhancement. The combined FSSs consisting of suitable units is necessary based on the consideration of the whole performance in three bands.

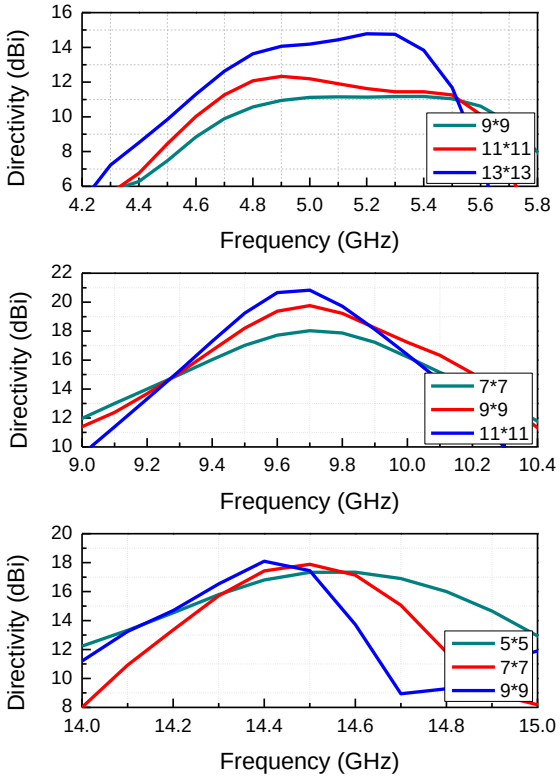

Fig. 8 Directivities in C, X and Ku bands with different units of combined FSS

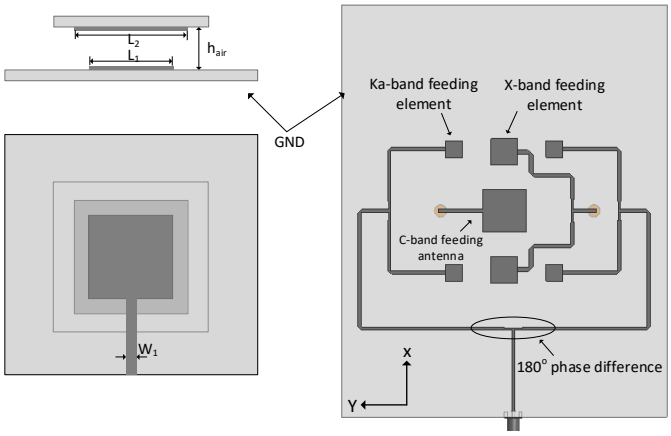

Fig. 9 The configuration of the feed unit and feed arrays

C. Feed Antenna

In our design, the estimated frequencies are 5 GHz, 9.6 GHz and 14.6 GHz, respectively. The maximum frequency ratio reaches approximately 3:1. It is a challenging task to achieve three resonances in a FPCA with such a large frequency ratio. For example, the dimension of the aperture reaches approximately 5.8 λ_{ku}×5.8 λ_{ku} at 14.6 GHz if the size of the aperture is selected as 2 λ_c×2 λ_c at 5.0 GHz. This aperture is large for higher frequency, which may worse the 3-dB radiation performance caused by non-uniform field distribution as study in previous section. However, it is small for lower frequency, leading to limited directivity enhancement. To solve this problem, a sparse array instead of a single feeding antenna in X and Ku bands can be employed since it can obtain more uniform aperture illumination [27]. Moreover, by using sparse arrays, thinning of the array elements can result in a simpler feed structure while still avoiding grating lobes. In addition, for a triple-band antenna with the shared-aperture, the phase centers of these three frequencies are desirable to be same.

Considered the above demands, the feed antenna composed of a C-band patch, 1×2 X-band patch array and 2×2 Ku-band patch array is designed. The configuration of the feed unit and array with feed network is shown in Fig. 9. The microstrip patch with parasitic patch is employed as the unit of the feed antennas. Rogers 4003C ($\varepsilon_r = 3.55$) with a thickness of 0.508 mm is chosen as the substrate. A driven patch is excited by coaxial cable. This patch is printed on the top side of the dielectric substrate of the ground plane. An air space is generated by the driven patch and a parasitic patch with the height of h_{air}. The dimensions of the feeding unit are based on the operating frequencies. The designed parameters of the feed units are shown in Table I.

To make the phase center consistent in C, X and Ku bands, the feed units are carefully arranged. The C-band patch is placed in the center of the ground plane. Two X-band antennas are mounted on the right and left side of the C-band one with the distance of 40 mm. Four Ku-band units are around the C-band patch. The spacing between each unit of the Ku-band feed array is 40 mm along x-direction and 20 mm along y-direction, respectively. To excite these antennas, the feed line of the C-band antenna is connected with the coaxial cable. The feed networks for X-band and Ku-band feed arrays are designed and printed on the top side of the ground plane's substrate, including a 1×2 power divider and two 1×2 power dividers, respectively. To achieve in-phase excitation in the Ku-band array, a 180° phase difference is designed in the Ku-band feed network.

D. Computed Results

The tri-band FPCA is carried out by combining the proposed two FSS layers with the feed antennas. The entire model is calculated by using the EM software CST Microwave studio. The combined FSS layers consist of 13 units in x-direction and 10 units in y-direction, respectively, with the lateral size of 130×100 mm^2. This dimension is approximately 2.3 λ×1.7 λ at 5.2 GHz, 4.2 λ×3.2 λ at 9.6 GHz and 6.4 λ×4.9 λ at 14.6 GHz, respectively. The size is chosen based on considering a practical design with edge effects, gain performance at the two frequencies and low-cost as well.

The simulated return losses of the proposed antenna are shown in Fig. 10, with the calculated results of the FPCA fed by simple patch in each band as comparison. The simulated S_{11} below -10 dB is from 5.0 GHz to 5.5 GHz, 9.67 GHz to 9.9 GHz and 14.45 GHz to 15.9 GHz when the cavity is excited by the single patch. A slight wider impedance matching is obtained when the feed network is integrated with the feed units, where the S_{11} below -10 dB is wider than approximately 100 MHz in X band and 90 MHz in Ku band, respectively.

TABLE I
DESIGNED PARAMTERS OF THE FEED UNITS

Feed units	W_1 (mm)	L_1 (mm)	L_2 (mm)	h (mm)
C-band	1.12	14.6	16.3	4
X-band	1.12	8.2	9	2
Ku-band	1.12	4.7	5.7	1

The computed directivity curves are plotted in Fig. 11. It can be observed that the maximum directivity of 13.6 dBi, 21.3 dBi and 22.4 dBi are predicted at 5.2 GHz, 9.7 GHz and 14.6 GHz, respectively. Table 2 shows the features of the overall design and the FPCA fed by simple patch in different apertures. Due to the larger aperture and more uniform aperture illumination caused by the sparse arrays, a higher directivity as well as the radiation bandwidth are obtained in X and Ku bands. It should be noted that the peak directivity of the overall design in C band is lower than the previous one in Section III (A). That is because the aperture of the overall design (10×13 units) is smaller than the one in that section, whose aperture consists of 13×13 units.

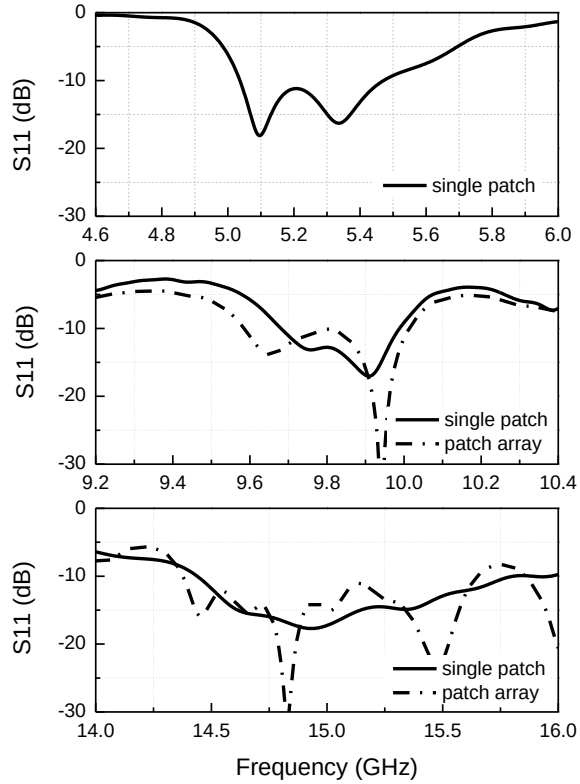

Fig. 10 Simulated S11of the proposed antenna fed by single patch and array

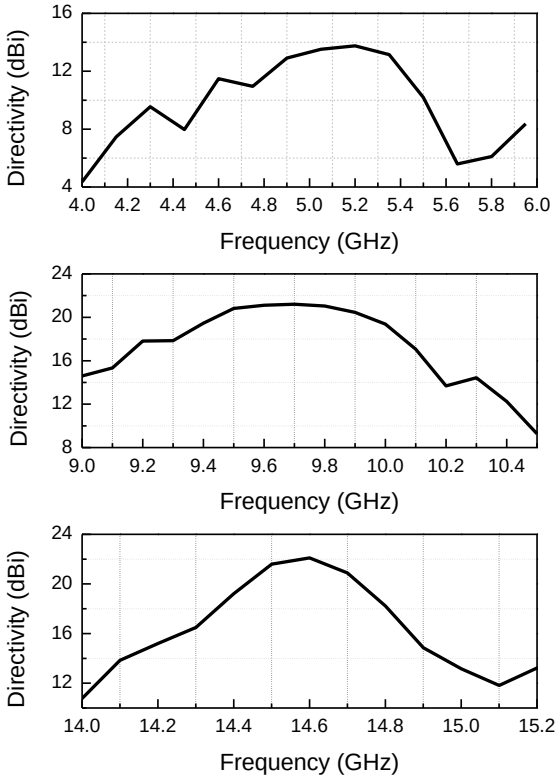

Fig. 11 Simulated directivity of the proposed antenna

IV. Experimental Results

Based on the discussion above, a prototype is fabricated as shown in Fig. 12. Four hexagonal nylon spacers are placed at four corners to support the suspended the two FSS layers and create an air-gap of 3.9 mm between the two FSS layers and 18.2 mm between the ground plane and the lower FSS layer, respectively. The overall profile of this antenna is 21 mm, which is approximately 1/3 λ at 5.2 GHz. Around 30% reduction of the cavity profile is obtained compared with a conventional FPCA. The feed units in C, X and Ku bands are supported by the foams with the thickness of 4mm, 2 mm and 1 mm, respectively. This foam can be seen as air approximately since its relative permittivity is similar to air. They are also modeled and taken into consideration during the design process of simulation. The lateral dimension of the antenna is of the same size of the FSS layers, which is 130 mm×100 mm.

TABLE II
Performance features of the overall design and the FPCA fed by simple patch

Operating band	Feed antenna	Aperture (units)	Peak directivity (dBi)	3-dB radiation bandwidth (%)
C	single	13×13	14.8	15.7
	single	10×13	14.6	13.8
X	single	11×11	21.2	5.2
	1×2 array	10×13	21.8	7.3
Ku	single	7×7	17.5	2.1
	2×2 array	10×13	22.3	2.4

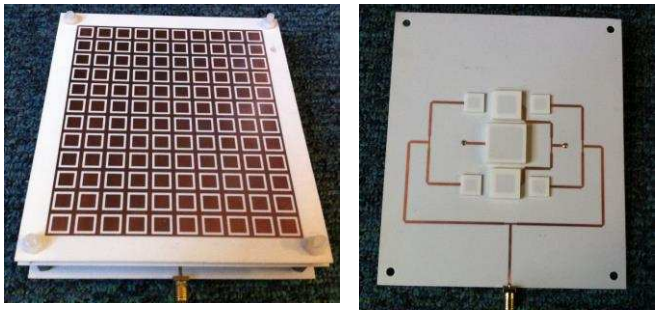

(a) (b)

Fig. 12 The prototype of the proposed antenna: (a) the whole antenna; (b) the feed antenna

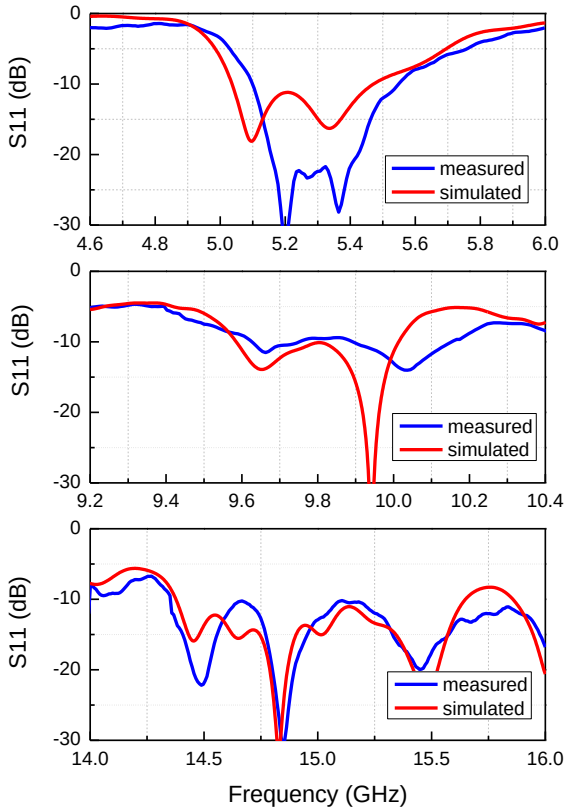

Fig. 13 Measured and simulated S parameters (Solid line; dashed line)

Fig. 13 shows the calculated and measured reflection coefficients of the proposed antenna. It can be found that this antenna works well in C, X and Ku bands as our expectation. The measured S_{11} below -10 dB is from 5.1 GHz to 5.5 GHz, 9.6 GHz to 10.2 GHz and 14.4 GHz to 16.0 GHz with the impedance bandwidth of 7.5%, 6.1% and 10.5% respectively. Some difference exists between the simulated and measured results, mainly due to the inaccuracies during the antenna fabrication and assembly.

The realized gain of this prototype is found by the gain comparison method, using a standard gain horn antenna with known gain, which is shown in Fig. 14. The gain at upper frequency is higher than the one at lower frequency since the electrical aperture of upper frequency is larger than the one of lower frequency. The measured peak gain occurs at 5.2 GHz, 9.7 GHz and 14.6 GHz, reaching 14.2 dBi, 18.9 dBi and 19.8 dBi, respectively. Compared with the simulated values, around 0.5 dB, 0.8 dB and 1.2 dB gain loss occurring in C, X and Ku bands is attributed to fabrication tolerances and cable loss when this antenna was tested. The measured 3-dB gain bandwidth reaches approximately 12%, 7.2% and 2.3% in C, X and Ku bands, respectively.

The radiation patterns were measured in anechoic chamber. In our measurement, the co-polar and cross-polar radiation patterns in E- and H- planes in the proposed three bands have been tested. All the measured results have a good agreement with the computed radiation patterns. The radiation patterns at 5.2 GHz, 9.6 GHz and 14.6 GHz are plotted in Fig. 15, Fig. 16 and Fig. 17, respectively, with the simulated results as comparison. It can be found that the peak radiation occurs in the broadside direction at these three frequencies. The sidelobe lower than -15 dB obtained in the whole operating frequencies. Moreover, a lower cross polarization over 35 dB is obtained as well.

Due to the symmetric configuration of the FSS structure, the polarization of this antenna can keep consistent with that of the feeding antenna, which implies that this radiation characteristic can easily altered by employing a feeding antenna with a different polarization. For instance, if a circularly polarized antenna is used as the feed, the radiation of this tri-band FPCA will also be circularly polarized.

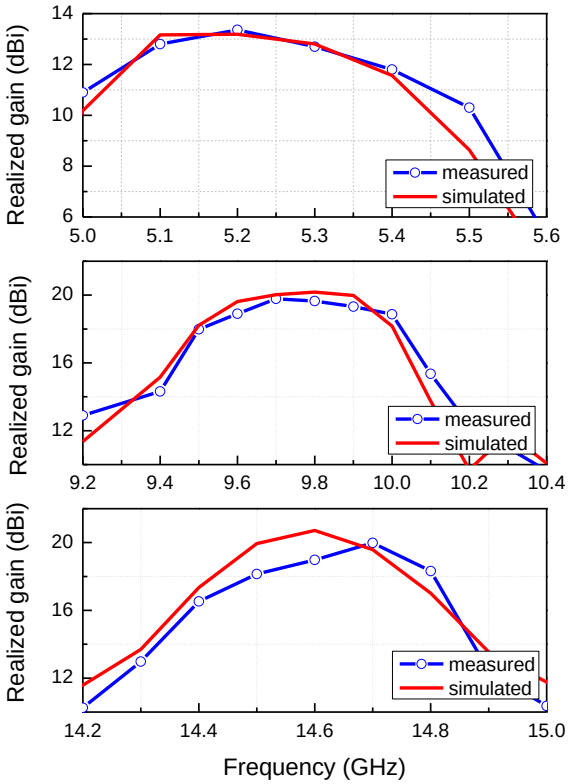

Fig. 14 Measured and simulated realized gain (Solid line; dashed line)

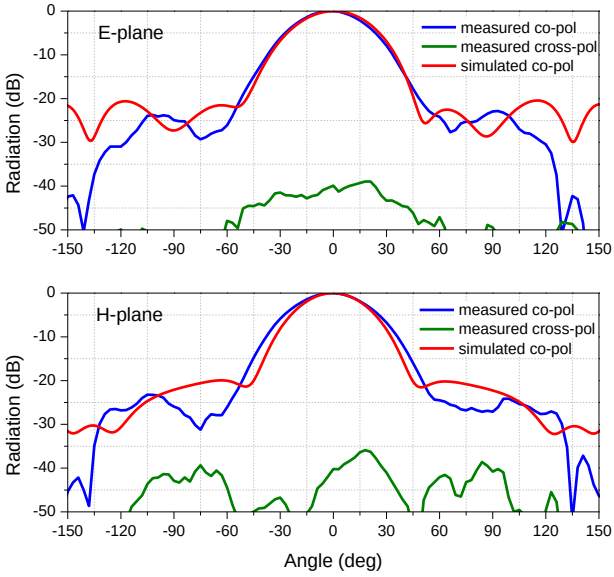

Fig. 15 Measured and simulated radiation patterns at 5.2 GHz

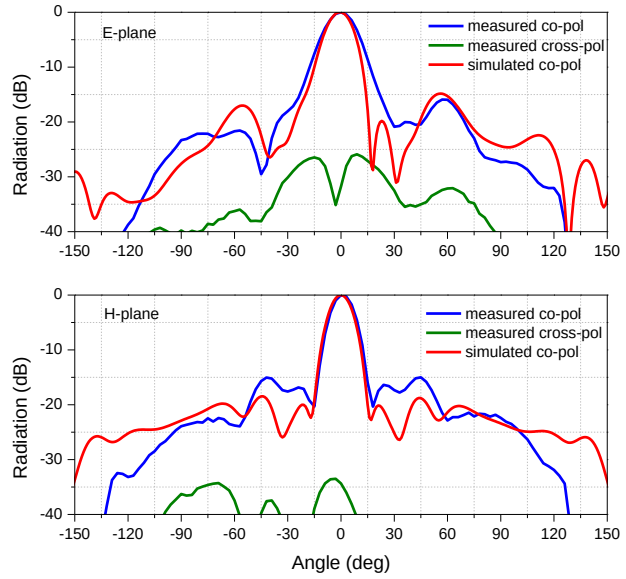

Fig. 16 Measured and simulated radiation patterns at 9.6 GHz

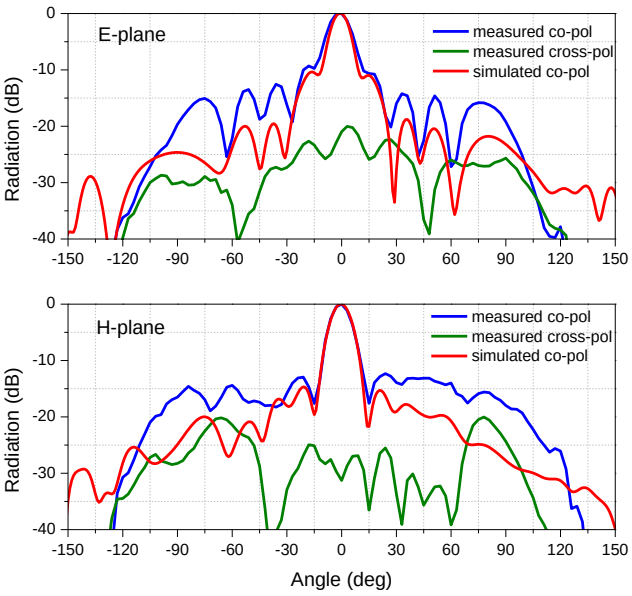

Fig. 17 Measured and simulated radiation patterns at 14.6 GHz

V. Conclusion

A low-profile tri-band FPCA operating in C/X Ku bands is presented. The working principle of this antenna is explained. Two FSS layers are employed as the PRS, which consist of a ring slot and two rings on the upper and lower layers, respectively. The high directivities in X-band and Ku band are attributed to the separate cavities formed by the lower and upper FSS layers, respectively and the third resonance is based on the combined FSS layer. The profile of this proposed antenna is only 1/3 wavelength at lower frequency. Compared with a conventional FPCA, the reduction of 30% of the antenna profile is achieved. This antenna also achieves a high frequency ratio approximately 3:1. To illuminate the cavity more uniformly, a C-band patch antenna surround by a simple 1×2 sparse X-band antenna array and 2×2 sparse Ku-band antenna array is applied as the primary source. A prototype is fabricated and measured. The experimental results have validated the design concept and indicate that tri-band gain enhancement can be achieved. The prototype gives measured peak gain of 14.2 dBi, 18.9 dBi and 19.8 dBi at 5.2 GHz, 9.6 GHz and 14.6 GHz, respectively, with the 3-dB gain bandwidth of 12%, 7.2% and 2.3%. The gain bandwidth can be well covered by the impedance bandwidth for the reflection coefficient below -10 dB in the three operating bands. This proposed antenna has obtained promising performance such as low-profile, tri-band, large frequency ratio, very simple feed network, easy fabrication and low-cost.

Acknowledgment

The authors thank the project of 'DIFFERENT' funded by EC FP7 (grant number: 6069923). Thank to Mr. Simon Jakes at the University of Kent for antenna fabrication.

References

[1] W. Imbriale, S. Gao and L. Boccia (eds), Space Antenna Handbook, John Wiley & Sons, UK, May 2012

[2] A. Pal, A. Mehta, D. Mirshekar-Syahkal, P. Deo, and H. Nakano, "Dual-Band Low-Profile Capacitively Coupled Beam-Steerable Square-Loop Antenna," Antennas and Propagation, IEEE Transactions on, vol. 62, pp. 1204-1211, 2014.

[3] M. Maqsood, S. Gao, T. W. Brown, M. Unwin, R. De Vos Van Steenwijk, J. Xu, and C. I. Underwood, "Low-cost dual-band circularly polarized switched-beam array for global navigation satellite system," IEEE Trans. Antennas Propag, vol. 62, pp. 1975-1982, 2014.

[4] Abutarboush, Hattan F., et al. "Compact printed multiband antenna with independent setting suitable for fixed and reconfigurable wireless communication systems." Antennas and Propagation, IEEE Transactions on60.8 (2012): 3867-3874.

[5] Anguera, Jaume, et al. "Dual-frequency broadband-stacked microstrip antenna using a reactive loading and a fractal-shaped radiating edge." IEEE Antennas and Wireless Propagation Letters 6 (2007): 309-312.

[6] Cao, Y. F., S. W. Cheung, and T. I. Yuk. "A Multiband Slot Antenna for GPS/WiMAX/WLAN Systems." Antennas and Propagation, IEEE Transactions on 63.3 (2015): 952-958.

[7] Luo, Qi, et al. "Design and Analysis of a Reflectarray Using Slot Antenna Elements for Ka-band SatCom." Antennas and Propagation, IEEE Transactions on 63.4 (2015): 1365-1374.

[8] Aboserwal, Nafati, Constantine Balanis, and Craig R. Birtcher. "Conical horn: Gain and amplitude patterns." Antennas and Propagation, IEEE Transactions on 61.7 (2013): 3427-3433.

[9] Yurduseven, Ozan, et al. "Parametric analysis of extended hemispherical dielectric lenses fed by a broadband connected array of leaky-wave slots." IET Microwaves, Antennas & Propagation 9.7 (2014): 611-617.

[10] Ye, S., Geng, J., Liang, X., Jay Guo, Y., & Jin, R. (2015). A Compact Dual-Band Orthogonal Circularly Polarized Antenna Array With Disparate Elements.Antennas and Propagation, IEEE Transactions on, 63(4), 1359-1364

[11] Moustafa, L., and B. Jecko. "EBG structure with wide defect band for broadband cavity antenna applications." Antennas and Wireless Propagation Letters, IEEE 7 (2008): 693-696.

[12] Orr, Robert, George Goussetis, and Vincent Fusco. "Design Method for Circularly Polarized Fabry–Perot Cavity Antennas." Antennas and Propagation, IEEE Transactions on 62.1 (2014): 19-26.

[13] Wang, Naizhi, et al. "Wideband fabry-perot resonator antenna with two complementary FSS layers." Antennas and Propagation, IEEE Transactions on62.5 (2014): 2463-2471.

[14] Trentini, Giswalt Von. "Partially reflecting sheet arrays." Antennas and Propagation, IRE Transactions on 4.4 (1956): 666-671.

[15] Wang, Naizhi, et al. "Wideband Fabry–Perot Resonator Antenna With Two Layers of Dielectric Superstrates." Antennas and Wireless Propagation Letters, IEEE 14 (2015): 229-232.

[16] Sun, Yong, et al. "Subwavelength substrate-integrated Fabry-Pérot cavity antennas using artificial magnetic conductor." Antennas and Propagation, IEEE Transactions on 60.1 (2012): 30-35.

[17] Zeb, Basit Ali, Nasiha Nikolic, and Karu P. Esselle. "A High-Gain Dual-Band EBG Resonator Antenna with Circular Polarization." Antennas and Wireless Propagation Letters, IEEE 14 (2015): 108-111.
[18] Ourir, A., A. De Lustrac, and J-M. Lourtioz. "Optimization of metamaterial based subwavelength cavities for ultracompact directive antennas." Microwave and optical technology letters 48.12 (2006): 2573-2577.
[19] Ourir, A., A. De Lustrac, and J. M. Lourtioz. "All-metamaterial-based subwavelength cavities for ultra-thin directive antennas." Appl. Phys. Lett 88: 084103-1.
[20] Ghasemi, Abdorasoul, et al. "High Beam Steering in Fabry–Pérot Leaky-Wave Antennas." Antennas and Wireless Propagation Letters, IEEE 12 (2013): 261-264.
[21] Pirhadi, Abbas, et al. "Design of compact dual band high directive electromagnetic bandgap (EBG) resonator antenna using artificial magnetic conductor." Antennas and Propagation, IEEE Transactions on 55.6 (2007): 1682-1690.
[22] Ge, Yuehe, Karu P. Esselle, and Trevor S. Bird. "A method to design dual-band, high-directivity EBG resonator antennas using single-resonant, single-layer partially reflective surfaces." Progress In Electromagnetics Research C13 (2010): 245-257.
[23] Zeb, Basit Ali, et al. "A simple dual-band electromagnetic band gap resonator antenna based on inverted reflection phase gradient." Antennas and Propagation, IEEE Transactions on 60.10 (2012): 4522-4529.
[24] Meng, Fanji, and Satish Sharma. "A Dual-Band High Gain Resonant Cavity Antenna with A Single Layer Superstrate." (2015).
[25] Moghadas, Hamid, Mojgan Daneshmand, and Pedram Mousavi. "A dual-band high-gain resonant cavity antenna with orthogonal polarizations." Antennas and Wireless Propagation Letters, IEEE 10 (2011): 1220-1223.
[26] Ge, Yuehe, and Can Wang. "A tri-band Fabry-Perot cavity for antenna gain enhancement." Antennas and Propagation Society International Symposium (APSURSI), 2013 IEEE. IEEE, 2013.
[27] Gardelli, Renato, Matteo Albani, and Filippo Capolino. "Array thinning by using antennas in a Fabry-Perot cavity for gain enhancement." Antennas and Propagation, IEEE Transactions on 54.7 (2006): 1979-1990.